3rd Intl. Conf. on Synchrotron Radiation in Materials Science
Singapore, 21-24 January 2002
Proceedings to be published in NIMB

Magnetism in heterogeneous thin film systems: Resonant X-ray scattering studies

J. B. Kortright,[1] J. S. Jiang,[2] S. D. Bader,[2] O. Hellwig,[3] D. T. Marguiles,[3] and E. E. Fullerton[3]

[1]*Materials Science Division, Lawrence Berkeley National Laboratory, Berkeley, CA 94720 USA*

[2]*Materials Science Division, Argonne National Laboratory, Argonne, IL 60439 USA*

[3]*IBM Almaden Research Center, 650 Harry Road, San Jose, CA 95120 USA*

Abstract

Magnetic and chemical heterogeneity are common in a broad range of magnetic thin film systems. Emerging resonant soft x-ray scattering techniques are well suited to resolve such heterogeneity at relevant length scales. Resonant x-ray magneto-optical Kerr effect measurements laterally average over heterogeneity but can provide depth resolution in different ways, as illustrated in measurements resolving reversible and irreversible changes in different layers of exchange-spring heterostructures. Resonant small-angle scattering measures in-plane heterogeneity and can resolve magnetic and chemical scattering sources in different ways, as illustrated in measurements of granular alloy recording media.

Keywords: magnetic films, exchange coupling, magnetic recording media, x-ray spectroscopy, X-ray scattering, magneto-optical effects

Magnetic thin film systems are of interest both because of their current and future technological applications and because they provide model systems to understand magnetic behavior and interactions. Advanced synthetic techniques allow controlled growth of a wide variety of systems. Common among most systems is magnetic and/or chemical heterogeneity that can manifest in many ways. Direct exchange between two magnetic layers and indirect exchange through a non-magnetic spacer layer are important effects of heterogeneity in layered systems. Basic atomic magnetic and chemical structure can be modified at interfaces of dissimilar materials. In-plane chemical segregation and lateral patterning are increasingly used to engineer magnetic correlation lengths, structure, and reversal behavior by altering the balance of different energies in the system. All of these phenomena result from heterogeneity occurring over length scales from atomic to tens of nanometers. Techniques able to resolve chemical and magnetic structure and interactions at these length scales should be extremely useful in understanding such systems.

This paper reviews two distinct but related magneto-optical (MO) techniques that use resonant soft x-rays to gain relevant spatial resolution, both in depth and laterally, in two very different types of magnetic systems. The soft x-ray spectral range from 500 eV to 2000 eV is especially useful for such studies because it contains relevant core levels both the 3*d* transition elements and 4*f* rare earth elements whose electronic structure is the source of magnetism [1]. The dipole transitions at these core resonances yield large, resonant enhancements in optical and magneto-optical properties that bring elemental chemical and magnetic sensitivity to several techniques capable of resolving heterogeneity at the nanometer level and above [1, 2].

Specifically we consider here the soft x-ray analogs of the MO Kerr effect (XMOKE) and small-angle scattering (SAS). MOKE and SAS are well-developed techniques in the near-visible and hard x-ray ranges, respectively, with experimental and theoretical formalisms that are readily extended into the soft x-ray range [2, 3, 4]. While both are scattering techniques, they have very different sensitivities to heterogeneity. XMOKE measures specularly reflected beams and hence laterally averages over in-plane heterogeneity, although it can provide valuable depth resolution as shown below. SAS measures diffuse scattering out of the forward scattered beam and is thus inherently sensitive to lateral heterogeneity.

Theoretical descriptions of XMOKE and resonant charge and magnetic x-ray scattering take different forms that can be shown to be equivalent in appropriate limits [2]. MOKE and XMOKE describe optical properties by the dielectric tensor that for cubic materials with magnetization M along z takes the form

$$\hat{\boldsymbol{\varepsilon}} = \begin{pmatrix} \varepsilon_{xx} & \varepsilon_{xy} & 0 \\ -\varepsilon_{xy} & \varepsilon_{xx} & 0 \\ 0 & 0 & \varepsilon_{zz} \end{pmatrix}. \quad (1)$$

Here off-diagonal elements result from spin-dependent MO effects and diagonal elements result primarily from spin-independent charge effects. While $\boldsymbol{\varepsilon}$ describes *bulk* properties, resonant x-ray scattering is described by an *atomic* scattering factor f. Using the formalism of Hannon, *et al.* [5],

$$f = (\mathbf{e}_\mathbf{f}^* \cdot \mathbf{e}_\mathbf{0}) f_c + i(\mathbf{e}_\mathbf{f}^* \times \mathbf{e}_\mathbf{0}) \cdot \mathbf{m} f_{m1} + (\mathbf{e}_\mathbf{f}^* \cdot \mathbf{m})(\mathbf{e}_\mathbf{0} \cdot \mathbf{m}) f_{m2}, \quad (2)$$

where $\mathbf{e}_\mathbf{0}$ and $\mathbf{e}_\mathbf{f}$ are polarization vectors of the incident and scattered radiation and $\mathbf{m}$ is a unit vector in the direction of local magnetization. Each term has a distinct polarization characteristic. f_c is non-resonant plus resonant charge scattering. f_{m1} is resonant magnetic scattering first order in $\mathbf{m}$ whose real and imaginary terms represent magnetic circular birefringence and dichroism, respectively. f_{m2} is resonant magnetic scattering 2nd order in $\mathbf{m}$ representing magnetic linear birefringence and dichroism. f_{m2} is small compared to f_{m1} for the ferromagnetic films studied here and is neglected.

In the following we review first XMOKE studies of exchange-spring heterostructures, and resonant SAS studies of magnetic and chemical heterogeneity in longitudinal recording media.

Resolving magnetic and chemical structure in depth is generally important in layered magnetic systems. Two examples include layered heteromagnetic films where direct exchange between antiferromagnetic and ferromagnetic layers yield exchange bias [6, 7], and between two ferromagnetic layers yield exchange hardening [8]. When different layers contain distinct magnetic elements XMOKE can be used to resolve magnetic interactions between layers and in-depth into structures.

Here we consider exchange-spring systems, of interest as a means of developing superior permanent magnets having higher energy product than currently available in nominally single-phase hard magnets [9]. Higher energy products can result from exchange coupling "soft" phases having high M but low anisotropy with "hard" phases having low M but high anisotropy [10]. Thin films provide well-defined systems to study exchange coupling between hard and soft phases [11], as in the exchange-spring system shown schematically in Fig. 1. Interfacial exchange modifies the field-dependent magnetic properties of each layer. When the soft layer is thick enough its top region is free to reverse in an applied field $|H| \geq |H_N|$ while its lower region at the interface resists complete reversal because of exchange coupling. The soft layer exerts a torque on the hard layer, whose top region near the interface responds by partially reversing. In an ideal system each layer responds homogeneously in-plane, and a Bloch domain wall or magnetization spiral in the film plane is nucleated at H_N. When reverse H is less than the hard layer's coercive field, H_{irr}, its removal allows the M spiral or spring to reversibly unwind. Only at sufficiently large $|H| > |H_{irr}|$ does the hard layer and the entire structure switch irreversibly.

Bulk magnetization measurements of exchange-spring systems observe two steps in hysteresis loops corresponding to reversible domain wall nucleation (at H_N) and irreversible hard layer reversal (at H_{irr}) as in Fig. 3c. While such loops can be fit by 1-D models of laterally uniform spins that vary only normal to the film [11], measurements sensing the aggregate moment leave unresolved some details of the individual hard and soft layer reversal. It is of interest to measure reversal behavior of the hard and soft layers separately. Ideally measurements would have depth resolution within each layer to reveal how the domain wall is partitioned between the two layers.

Using an exchange-spring system MgO/Cr(20 nm)/Sm-Co(20 nm)/Fe(20 nm)/Cr(5 nm) grown on an MgO (110) substrate, we have previously reported on a detailed XMOKE study of the soft Fe layer using x-rays tuned near the Fe L_3 core level at 707 eV [3]. Combined XMOKE intensity and rotation measurements resolve changes in the net longitudinal and transverse Fe moments during reversal, with the net transverse moment resulting from the M spiral in Fig. 1. Furthermore, this study showed that by tuning photon energy just several eV across the L_3 line we can significantly alter the x-ray penetration

depth into the Fe, confirming that it is the top of the soft Fe layer that reverses at H_N and the bottom that resists reversal until H reaches H_{irr}. These results are in qualitative agreement with a 1-D model of the spin spiral from ref. 8. We could not sense the Sm-Co layer by tuning to the Co L_3 line of this sample, because its large roughness reduced specular reflectivity below the threshold of the diode detector at the high incidence angle q needed for significant x-ray penetration to that layer.

A smoother Sm-Co/Fe sample has since allowed us to begin to isolate the hard layer reversal. Also grown on MgO (110) as MgO/Fe(20 nm)/Sm-Co(80 nm)/Fe(20 nm)/Ag(20 nm), we study the top of two exchange-coupled interfaces in this sample. At q = 8° strong Co $L_{2,3}$ resonant features are observed in Kerr intensity spectra (Fig. 2), indicating clear sensitivity to Co magnetization associated with the Sm-Co layer. XMOKE intensity hysteresis loops measured at the L_3 peak (778.5 eV) using elliptical polarization are shown in Fig. 3 a & b. A major and a minor loop are shown, each starting and ending at positive H. The major loop shows clear hysteresis of longitudinal Co moment indicating that negative saturation was reached. Note that the onset of Co reversal occurs at H_N where the domain wall forms, and there is no change in Co signal at H_{irr} where the hard layer is known to reverse from the SQUID loop in Fig 3c. The minor loop, measured after positive saturation, shows entirely reversible motion of Co in a range of reverse H less than H_{irr}.

These Co XMOKE loops reveal directly that part of the Sm-Co layer near the interface participates in the reversible exchange-spring mechanism, *i.e.*, that the domain wall extends well into the hard layer. The absence of Co XMOKE signal change at H_{irr} reveals that the domain wall extends into the hard layer at least several times the x-ray skin depth in that layer at the peak of Co L_3 line, which is estimated to be ~ 2 nm at q = 8°. By varying skin depth in the Sm-Co layer with energy [3] and angle tuning, future experiments should more fully depth-resolve magnetic reversal behavior of the Sm-Co layer. Similar exchange softening of the hard layer has been inferred from related XMOKE studies in the FePt/NiFe hard/soft exchange-spring system [12]. This ability to selectively probe the reversal behavior of deeply buried layers is important in the study of many layered heteromagnetic systems.

Lateral heterogeneity in magnetic thin films is ubiquitous. Even in films that are nominally chemically homogeneous, magnetic structure during reversal presents heterogeneity. Polycrystalline grain structure and surface roughness can interact with magnetization. Chemical segregation in polycrystalline alloy films forms the basis of magnetic recording media, and laterally patterned and self-assembled nanoparticle magnetic films are of great current interest.

Current magnetic recording media consists of chemically segregated, polycrystalline grains whose grain-centers are ferromagnetic with in-plane anisotropy and whose grain boundaries are nominally non-magnetic [13]. This chemically and magnetically heterogeneous thin film microstructure has evolved through several generations of recording media via an increasingly complex set of alloys including CoCr, CoPtCr, and CoPtCrB. In this progression the additives Cr and later B are known to segregate to and produce nonmagnetic grain boundary phases that have been thought to reduce exchange coupling between adjacent grains, thereby enabling sharper bit transitions and higher recording density [14]. The chemical heterogeneity associated with these films is resolved using standard high-resolution techniques such as TEM and micro-EELS [15]. It has remained difficult, however, to directly measure magnetic correlation lengths giving the distance over which grain-to-grain magnetism is correlated.

We have found that both magnetic and chemical heterogeneity in recording media films are strong scattering sources when tuned to specific soft x-ray core resonances to enhance contrast [16, 17]. This transmission SAS technique positions the scattering vector q in the film plane to optimize coupling to in-plane structure [4]. While long soft x-ray wavelengths limit the maximum q, structural information with resolution down to 1 nm is available.

Scattering vs. q from an as-deposited $Co_{69}Pt_9Cr_{22}$ media film measured near the Co and Cr L_3 lines is shown in Fig. 4. Two distinct peaks are observed, with the higher q peak prominent at both Co and Cr L_3 lines and the lower q peak much more pronounced at the Co than the Cr resonance. The presence of each peak indicates a dense arrangement of scattering centers in the film plane with average nearest neighbor spacing given by roughly $2\pi/q_{peak}$. The $q = 0.06$ Å^{-1} peak corresponds to a spacing of 10.5 nm, while $q = 0.014$ Å^{-1} peak corresponds to a spacing of 45 nm. The known size scale of Cr grain

boundary segregation is roughly 10 nm [15], and Cr XMCD measurements reveal that it shows very little net moment in these alloys. Thus we expect resonant scattering enhancements at the Cr L_3 line to result primarily from regions defined by Cr chemical segregation. The position of the high q peak is entirely consistent with this interpretation.

Co resonant scattering is expected to include chemical scattering from Co segregation to grain centers with the same length scale as Cr segregation, and additionally magnetic scattering from magnetic correlation lengths that could be as short as the grain size or larger if the magnetization of adjacent grains is partially correlated. The high q peak in the Co scan is thus interpreted to result from chemical scattering plus possible magnetic scattering. The 45 nm spacing is clear evidence of a well-defined magnetic correlation length several times larger than the chemical grain size. Interference between chemical and magnetic scattering amplitudes is also possible [4, 17,18], and expected to be more pronounced in the region between the peaks and at the high q peak. The Co and Cr resonant scans in Fig. 4 are vertically scaled to match at high q. Their difference (open circles) is thus expected to roughly reflect magnetic correlation lengths and charge-magnetic interference scattering.

The above interpretation of magnetic and chemical peaks is qualitative. One approach to independent, quantitative determination of the scattering sources contributing to the peaks is to model the energy spectra of the scattering at each peak [4, 17]. Measured Co L_3 energy spectra at these two peaks are shown as symbols in Fig. 5, and clearly have very different shape. Modeling these resonant shapes requires measured values of f_c and f_{m1} for Co. These were obtained from transmission absorption measurements of the saturated media film with linear and circular polarization, followed by Kramers-Kronig transformation of the imaginary part of these quantities to obtain their real parts [2]. Non-resonant f values for Cr and Pt were taken from tabulated values [19].

Following standard SAS formalisms, the amplitude for different scattering sources is given by the difference of amplitudes of the two phases defining the heterogeneity. The simplest model for pure magnetic scattering yields amplitude proportional to f_{m1} of Co [4, 17]. The corresponding intensity is

scaled and plotted in Fig. 5, with a small non-resonant background added. The good agreement of model and measured spectra confirms the magnetic origin of the low-q peak and thus that magnetic correlation lengths in this sample are several times the chemical grain size.

Modeling the high-q spectrum requires postulating compositions of the segregated phases at the grain boundaries and centers, forming the appropriate scattering amplitudes of these two phases as linear combinations of elemental scattering factors, and squaring the difference of these amplitudes to obtain the intensity spectrum. A model spectrum is scaled and plotted with the high-q data in Fig. 5. The Co-rich (magnetic) phase in this model assumes Co:Pt:Cr ratio of 20:2:1, while the Cr-rich (grain boundary) phase has Co:Cr ratio of 1:1. Model spectral shapes are quite sensitive to the compositions of the different phases, and models with strong scattering Pt in both phases significantly degrade agreement. The high-q peak can thus be modeled as pure chemical scattering, as expected. This model does not provide a unique determination of composition of the segregated phases, and refinements need to include density differences, mass conservation, and possible charge-magnetic interference more carefully. However it is clear that the spectral modeling approach is a powerful tool not only to resolve magnetic from chemical scattering, but also to provide some idea of the chemical make-up of nanoscale segregated phases.

In summary, soft x-ray resonant charge and magnetic scattering enhancements are large enough so that they can be used in straightforward ways to resolve chemical and magnetic structure and interactions at the nanometer length scale and above. Specular XMOKE measurements average laterally but can provide depth resolution in layered films. Diffuse scattering probes heterogeneity in the film plane. The two magnetic thin film systems reported on here are widely different in nature. This underscores the applicability of these techniques to a wide variety of systems.

Acknowledgements

Experiments were done at the Advanced Light Source at LBNL using beamlines 4.0, 8.0, and 6.3.2, where we acknowledge assistance from E. Arenholz, A. T. Young, E. M. Gullikson, and J. Denlinger.

Work at LBNL and ANL was supported by the U.S. Department of Energy, Basic Energy Sciences – Materials Sciences, under Contracts No. DE-AC03-76SF00098 and W-31-109-ENG-38, respectively.

References

[1] J. B. Kortright, D. D. Aswchalom, J. Stöhr, S. D. Bader, Y. U. Izderda, S. S. P. Parkin, I. K. Schuller, H.-C. Siegmann, J. Magn. Magn. Mat. 207 (1999) 7.

[2] J. B. Kortright, S.-K. Kim, Phys. Rev. B 62 (2000) 12216.

[3] J. B. Kortright, S.-K. Kim, E. E. Fullerton, J. S. Jiang, S. D. Bader, Nucl. Instrum. Meth. A 467-468 (2001) 1396.

[4] J. B. Kortright, S.-K. Kim, G. P. Denbeaux, G. Zeltzer, K. Takano, E. E. Fullerton, Phys. Rev B 64 (2001) 092401.

[5] J. P. Hannon, G. T. Trammel, M. Blume, D. Gibbs, Phys. Rev. Lett. 61 (1988) 1245; 62 (1989) 2644(E).

[6] J. Nogues, I. K. Schuller, J. Magn. and Magn. Mater. 192 (1999) 203.

[7] A. E. Berkowitz, K. Takano, J. Magn. and Magn. Mater. 200 (1999) 552.

[8] E. E. Fullerton, J. S. Jiang, S. D. Bader, J. Magn. and Magn. Mater. 200 (1999) 392.

[9] E. F. Keller, R. Hawig, IEEE Trans. Mag. 27 (1991) 3588.

[10] R. Skomski, J. M. D. Coey, Phys. Rev. B 48 (1993) 15812.

[11] E. E. Fullerton, J. S. Jiang, M. Grimsditch, H. C. Sowers, S. D. Bader, Phys. Rev. B 58 (1998) 12193.

[12] O. Hellwig, J. B. Kortright, K. Takano, E. E. Fullerton, Phys. Rev. B 62 (2000) 11694.

[13] H. N. Bertram, Theory of Magnetic Recording (Cambridge University Press, Cambridge, U.K.) 1994.

[14] M. Doerner, X. Bian, M. Madison, K. Tang, Q. Peng, A. Polcyn. T. Arnoldussen, M. F. Toney, M. Mirzamaani, K. Takano, E. E. Fullerton, D. Margulies, M. Schabes, K. Rubin, M Pinarbasi, S. Yuan, M. Parker, D. Weller, IEEE Trans. Magn. 37 (2001) 1052.

[15] M. Doerner, K. Tang, T. Arnoldussen, H. Zeng, M. F. Toney, D. Weller, IEEE Trans. Magn. 36 (2000) 43.

[16] O. Hellwig, D. T. Marguiles, B. Lengsfield, E. E. Fullerton, J. B. Kortright, Appl. Phys. Lett. 80 (2002) 1234.

[17] J. B. Kortright, O. Hellwig, D. T. Marguiles, E. E. Fullerton, J. Magn. and Magn. Mater. 240 (2002) 325.

[12] R. M. Osgood III, S. K. Sinha, J. W. Freeland, Y. U. Idzerda, S. D. Bader, J. Magn. Magn. Mater. 198 (1999) 698.

[19] B. L. Henke, E. M. Gullikson, J. C. Davis, At. Data Nucl. Data Tables 54 (1993) 181; and at http:/www-cxro.lbl.gov/optical_constants/.

Figure Captions

Figure 1. Schematic of an exchange-spring system consisting of a soft magnetic layer exchange-coupled to a hard magnetic layer. When a reverse field H opposes the saturation direction it causes the top of the soft layer to reverse forming a magnetization spiral or domain wall in depth into the system (arrows). This spiral magnetization structure is reversible until H is sufficient to cause the hard layer to reverse

Figure 2. Kerr intensity spectra from a Sm-Co/Fe exchange-spring sample across the Co $2p$ levels reveal clear sensitivity to Co in the buried Sm-Co layer. Spectra measured with opposite helicity elliptical polarization and saturated sample reveal characteristic asymmetry indicating sensitivity to the longitudinal moment of Co in the hard layer.

Figure 3. Kerr intensity hysteresis loops measured with x-rays tuned to the Co L_3 line are in (a) and (b), and reveal how part of the hard Sm-Co layer in the exchange-spring system responds to applied fields. (a) is a major loop, while (b) is a minor loop after positive saturation. (c) shows a SQUID major half loop of the same sample, with two-step reversal corresponding to reversible nucleation of the domain wall at H_N and the irreversible reversal of the hard layer at H_{irr}. All loops start at positive H.

Figure 4. Resonant q scans measured with x-ray energy tuned to the Co and Cr L_3 lines scaled to match at high q, and their difference. Two peaks indicate two correlation lengths in the film plane resulting from chemical segregation and magnetic correlation between grains. Lines connect data points.

Figure 5. Symbols are energy spectra across the Co L_3 line measured at the two different peaks in Fig. 4. Lines are model spectra based on measured Co resonant scattering factors that confirm the magnetic and chemical origin of the low and high q peaks, respectively.

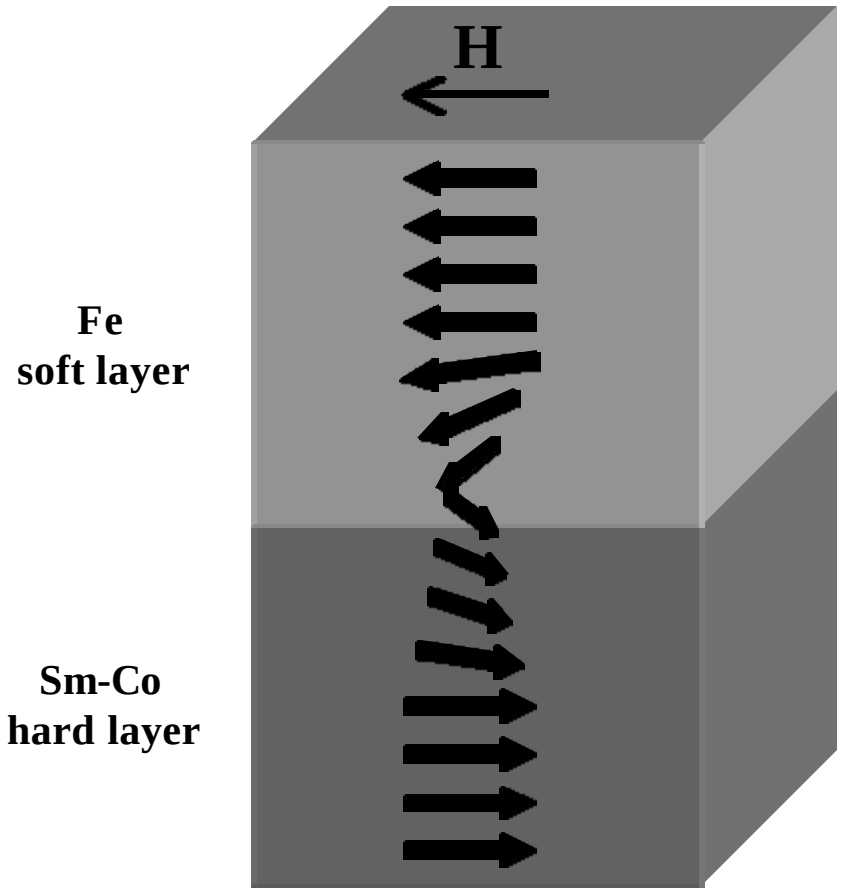

Figure 1

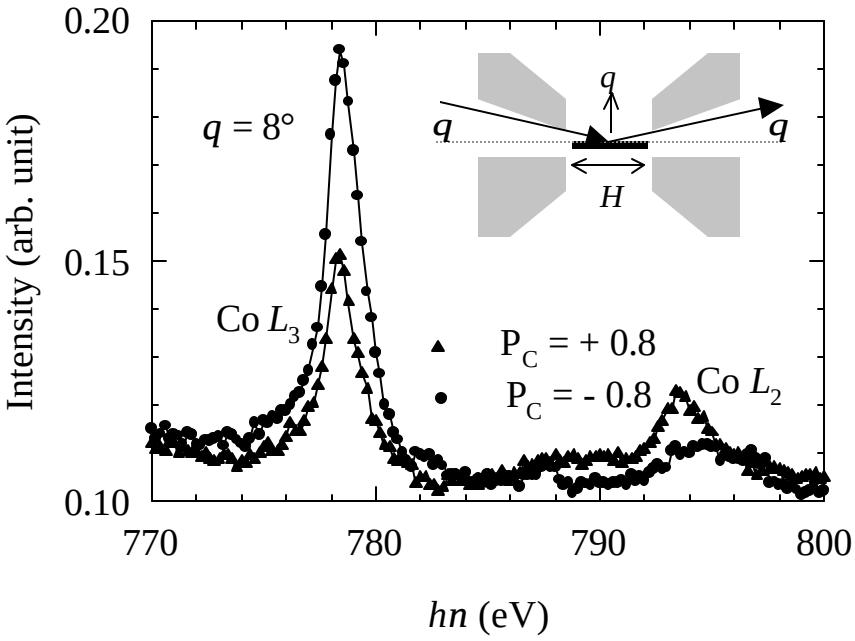
0.20
0.15
0.10
Intensity (arb. unit)
770
780
790
800
hn (eV)
q = 8°
Co L3
Co L2
P_C = + 0.8
P_C = - 0.8
q
q
q
H

Figure 2

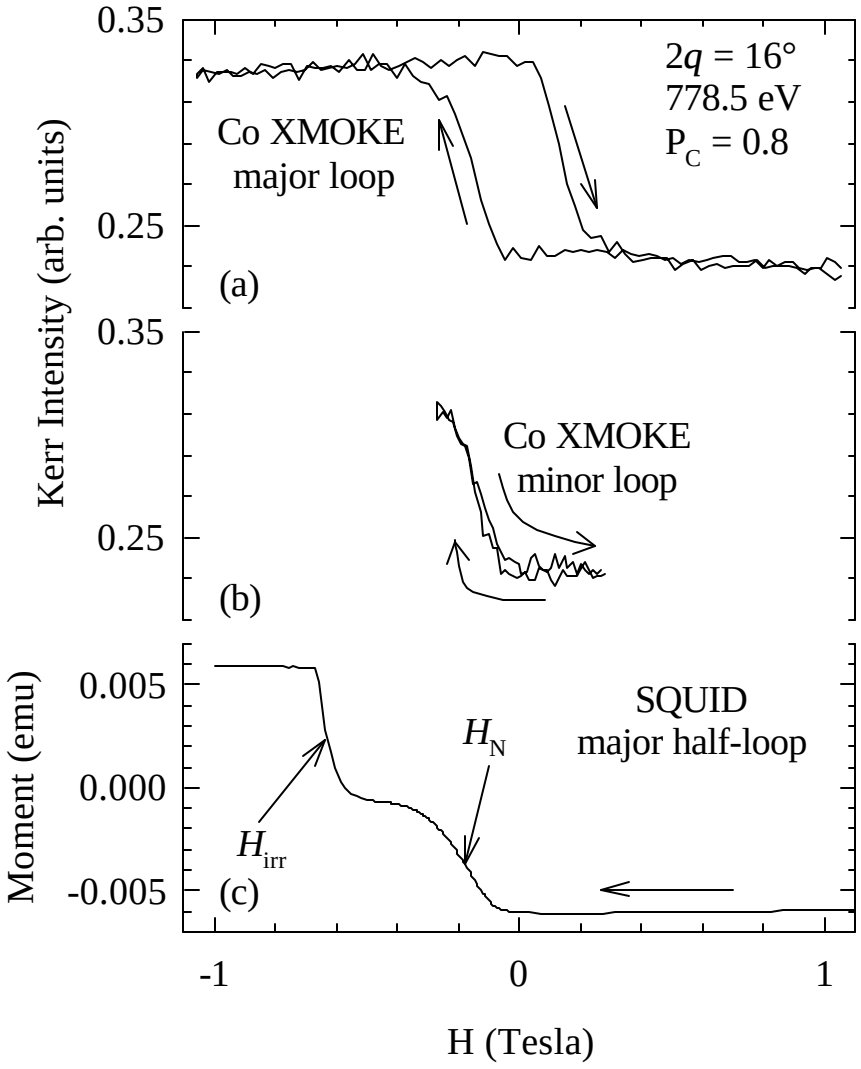
0.35
0.25
Kerr Intensity (arb. units)
2q = 16°
778.5 eV
P_C = 0.8
Co XMOKE
major loop
(a)
0.35
0.25
Co XMOKE
minor loop
(b)
Moment (emu)
0.005
0.000
-0.005
SQUID
major half-loop
H_N
H_irr
(c)
-1
0
1
H (Tesla)

Figure 3

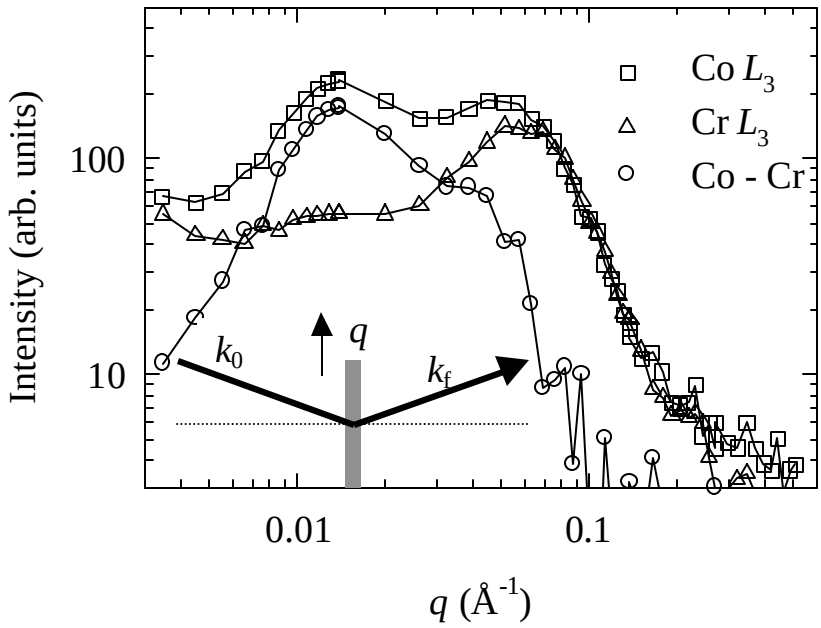

Figure 4

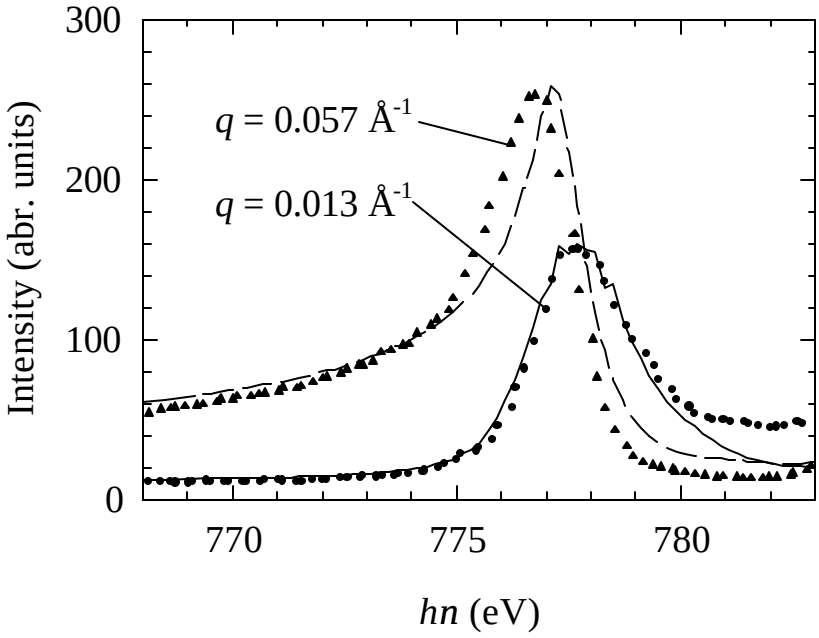
300
200
100
0
Intensity (abr. units)
q = 0.057 Å-1
q = 0.013 Å-1
770
775
780
hn (eV)

Figure 5